Flexible Mixed-Potential-Type (MPT) NO$_2$ Sensor Based on An Ultra-Thin Ceramic Film

Rui You [1,2], Gaoshan Jing [1,2,*], Hongyan Yu [1,2] and Tianhong Cui [3,*]

[1] State Key Laboratory of Precision Measurement Technology and Instruments, Tsinghua University, Beijing 100084, China; your13@mails.tsinghua.edu.cn (R.Y.); yuhongyan@mail.tsinghua.edu.cn (H.Y.)

[2] Department of Precision Instrument, Tsinghua University, Beijing 100084, China

[3] Department of Mechanical Engineering, University of Minnesota, Minneapolis, MN 55455, USA

[*] Correspondence: gaoshanjing@mail.tsinghua.edu.cn (G.J.); tcui@me.umn.edu (T.C.);
Tel.: +86-10-6278-7338 (G.J.); +1-612-626-1636 (T.C.)

Abstract: A novel flexible mixed-potential-type (MPT) sensor was designed and fabricated for NO$_2$ detection from 0 to 500 ppm at 200 °C. An ultra-thin Y$_2$O$_3$-doped ZrO$_2$ (YSZ) ceramic film 20 μm thick was sandwiched between a heating electrode and reference/sensing electrodes. The heating electrode was fabricated by a conventional lift-off process, while the porous reference and the sensing electrodes were fabricated by a two-step patterning method using shadow masks. The sensor's sensitivity is achieved as 58.4 mV/decade at the working temperature of 200 °C, as well as a detection limit of 26.7 ppm and small response time of less than 10 s at 200 ppm. Additionally, the flexible MPT sensor demonstrates superior mechanical stability after bending over 50 times due to the mechanical stability of the YSZ ceramic film. This simply structured, but highly reliable flexible MPT NO$_2$ sensor may lead to wide application in the automobile industry for vehicle emission systems to reduce NO$_2$ emissions and improve fuel efficiency.

Keywords: flexible mixed-potential-type (MPT) sensor; ultra-thin ceramic film; mesoporous TiO$_2$

1. Introduction

Air pollution from car exhaust has caused plenty of environmental disasters in several countries and affected a large number of lives around the world due to the rapid development of the automobile industry [1,2]. In particular, nitrogen oxides gases (NO/NO$_2$), as harmful gas pollutants, cause a variety of adverse health issues such as bronchitis, serious neurodegenerative diseases, and cancers [3]. These toxic gases also lead to urban environmental pollution issues such as acid rain and chemical smog [4]. To accurately and precisely monitor the NO$_X$ gases, especially NO$_2$, from car exhaust in a harsh working environment with a high temperature and large vibration, a high-performance NO$_2$ sensor was in high demand for vehicle emission systems to reduce NO$_2$ emissions and improve vehicle fuel efficiency.

A few NO$_2$ sensors have been developed based on various sensing techniques, including metal oxide semiconductor sensing [5,6], infrared light absorption [7,8] and electrochemical reaction [9–11]. Among these sensors, one type of electrochemical NO$_2$ sensor, mixed-potential-type (MPT) NO$_2$ sensor based on Y$_2$O$_3$-doped ZrO$_2$ (YSZ) solid electrolyte material, is widely investigated for a vehicle emission systems due to the sensor's excellent chemical and thermal stability at high working temperatures [12,13]. A typical MPT NO$_2$ sensor includes several functional layers: a bulk substrate; a heating electrode layer to let the sensor working at an appropriate temperature; a YSZ solid electrolyte layer; a reference electrode layer, and; a sensing electrode layer on top of the YSZ layer [14,15]. NO$_2$ gases' reaction with oxygen in the ambient environment occurs at the triple-phase-boundary (TPB) interface between the YSZ solid electrolyte layer and the sensing electrode layer. Eventually, the

electrochemical potential difference between the reference electrode layer and the sensing electrode layer is measured and correlated with the NO_2 gases concentration [16,17].

The MPT NO_2 sensor based on various sensing electrode materials has been developed to detect NO_2 gas. A composite material of In_2O_3 and MoO_3 has been utilized as the sensing material for NO_2 detection. With the MoO_3 doping ratio optimized at 5 wt%, the largest sensitivity of 59 mV/decade for NO_2 was achieved in the range of 10–200 ppm at 500 °C [18]. Another new type of composite oxide $Co_3V_2O_8$ mixed with YSZ particles was used as the NO_2 gases sensing material for an MPT sensor. With the mixture ratio between $Co_3V_2O_8$ mixed and YSZ particles configured at 60:40, the largest sensitivity of 81 mV/decade for NO_2 was achieved in the range of 10–400 ppm at 700 °C [19]. To further increase MPT sensors' sensitivity, various techniques have been applied to increase the sensing material's area, including etching the YSZ substrate surface using the hydrofluoric acid and template method with a self-assembled polystyrene sphere [20,21]. Due to the complexity of an MPT NO_2 sensor, several crucial steps to fabricate an MPT NO_2 sensor are realized manually and greatly affect the sensor's reliability and uniformity. In particular, the YSZ solid electrolyte layer needs to be fabricated as a functional layer with the thickness delicately controlled on a bulk substrate for all of these sensors. Moreover, an MPT sensor is usually placed close to a car engine and its working temperature is well above 600 °C, with high power consumption and a low shelf life. While it is also desirable to install an MPT sensor inside a low-temperature region of an exhaust pipe (100–300 °C) to monitor NO_2 emissions, such a disadvantage greatly limits the application of conventional MPT NO_2 sensors.

In this paper, a novel flexible mixed-potential-type (MPT) sensor based on an ultra-thin ceramic film was developed and utilized to detect NO_2. As shown in Figure 1, the sensor is composed of a heating electrode, a reference electrode, an NO_2 sensing electrode on the back side and front side of an ultra-thin 3 mol% Y_2O_3-doped ZrO_2 (YSZ-3Y) film 20 μm thick, respectively. The heating electrode was fabricated by a conventional lift-off process, while the porous reference and sensing electrodes were fabricated by a two-step patterning method using shadow masks. Due to the ceramic film's low thermal conductivity and thin film thickness, a low power assumption of 1025 mW was consumed to reach 246 °C in an area of 8.0 mm by 6.4 mm. The sensor's sensitivity could be achieved as 58.4 mV/decade at a working temperature of 200 °C. Additionally, the flexible sensor demonstrates superior mechanical stability after bending over 50 times due to the mechanical stability of the YSZ ceramic film. This flexible mixed-potential-type (MPT) sensor could be installed on an exhaust pipe's circular surface without interfering with exhaust emission and could monitor the NO_2 emission in a low-temperature region from 100 °C to 300 °C. This simple structured flexible MPT NO_2 sensor fabricated by highly reliable methods exhibits excellent performance to detect NO_2, which may lead to wide application in the automobile industry for vehicle emission systems to reduce vehicle emissions and improve fuel efficiency.
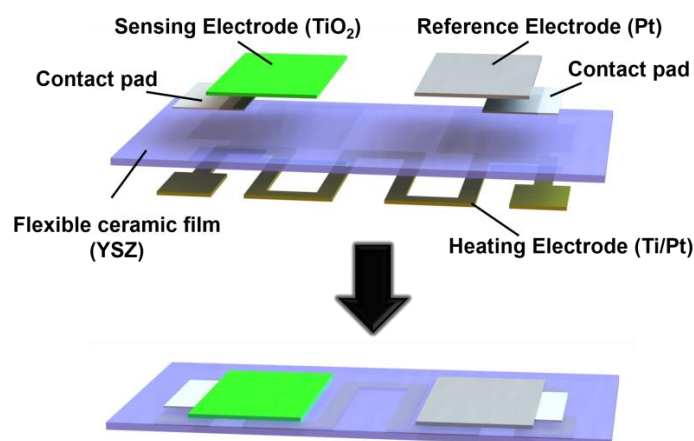

Figure 1. Schematic diagram of a flexible mixed-potential-type (MPT) NO_2 sensor.

2. Materials and Methods

2.1. Sensor Design and Simulation

The MPT NO_2 sensor's heating electrode was designed and its electrothermal performance was simulated by COMSOL Multi-physics software (COMSOL Inc., Los Angeles, CA, USA). The heating electrode's schematic diagram is illustrated in Figure 2 with two components: a YSZ based ultra-thin flexible ceramics film 20 μm thick, and; a Ti/Pt heating electrode. The heating electrode's key design parameters are listed in Table 1, the heating electrode's length is 94.8 mm with a width of 100 μm and a thickness of 4500 Å (500 Å Ti/ 4000 Å Pt). An adjustable driving voltage at 1 V–35 V was applied to the contact pads to investigate the electrothermal response of the heating electrode. In the heat transfer process, the ambient environment temperature was configured as 26 °C. It should be noted that the thermal conduction coefficient of the ceramic thin film is 2.7 $m^{-1} \cdot K^{-1}$ according to technical information provided by the flexible YSZ ceramic film's manufacturer [22], while Ti and Pt's material parameters are from the COMSOL library.
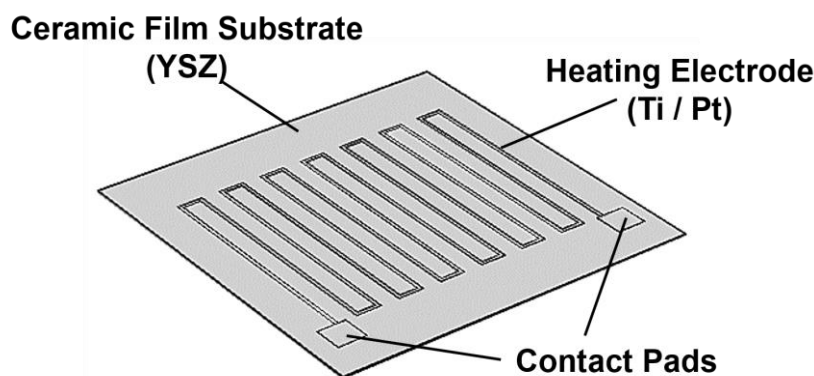

Figure 2. Geometry model of the sensor's heating electrode for stimulation by COMSOL Multiphysics.

Table 1. Design parameters and dimension of the sensors' heating electrode.

Parameters	Value
3 mol% Y_2O_3-doped ZrO_2 (YSZ-3Y) substrate	10 mm × 10 mm × 20 μm
Thickness of heating resistors (Å)	500 (Ti) / 4000 (Pt)
Heating electrode (μm)	94800 × 100 × 0.45
Driving voltage (V)	1–35 V
Thermal conduction coefficient (YSZ-3Y substrate) ($W \cdot m^{-1} \cdot K^{-1}$)	2.7
Ambient environment temperature (°C)	26 (air)

2.2. Device Fabrication

The NO_2 sensor was fabricated on a planar yttria-stabilized zirconia (YSZ) ceramic thin film (EnrG Inc., Buffalo, NY, USA) with two major processes. One is a lift-off process to fabricate a heating electrode, and the other is a two-step patterning process using shadow masks to fabricate the sensing and reference electrodes. The YSZ ceramic thin film was sandwiched between the heating electrode on the backside of the film and reference/sensing electrodes on the front side of the film.

As shown in Figure 3, the heating electrode was fabricated by a lift-off process. First, a thin layer of photoresist (1.6 μm, LOR 5B, Microchem Corp., Westborough, MA, USA) was spin coated on a four-inch silicon wafer. Then the YSZ ceramic film was positioned on the wafer surface guided by a laser marker and fixed on the silicon substrate by drying the photoresist at 190 °C for 180 s. Next, the second and third layers of photoresist (1.6 μm, LOR 5B, Microchem Corp., Westborough, MA, USA; 1.4 μm, AZ5214e, MicroResist, Berlin, Germany) were deposited on the fixed YSZ film surface by spin coating sequentially and soft baked at 190 °C and 105 °C for 180 s, respectively. The photoresist

films were exposed to UV light for 6 s using a mask aligner and developed for 90 s (MA150e, SUSS, MicroTec, Garching, Germany). Sequentially, 500 Å titanium and 4000 Å platinum metal layers were deposited by sputtering (904i, KDF Inc., Torrance, NJ, USA).
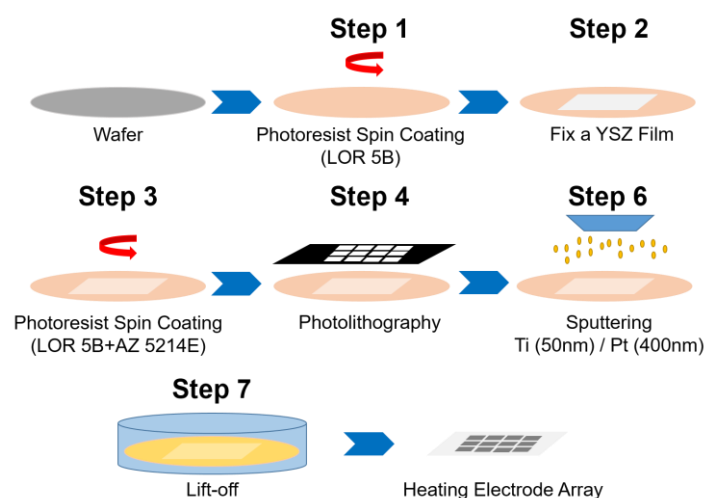

Figure 3. Schematic diagram of the fabrication process for the sensor's heating electrode.

Once the heating electrode was fabricated, the YSZ ceramic film with the heating electrode was flipped over and the reference electrode and the sensing electrode were fabricated on the front side of the film by a two-step patterning process using shadow masks, as shown in Figure 4. Thin and flexible PVC (Polyvinyl chloride) films were utilized as shadow masks for patterning the reference and sensing electrodes. First, PVC films were patterned by a laser cutter. Then the first PVC film was rolled and attached on the YSZ ceramic surface manually without generating bubbles aided by the electrostatic adhesion between the PVC film and YSZ substrate. The Pt reference electrode (RE) (2.0 mm × 6.0 mm) and the square-shaped platinum pad (1.0 mm × 2.0 mm) on the YSZ film were patterned by printing manually using platinum paste (Sino-platinum Metals Co., KunMing, China.). Next, the PVC film was removed and the film with Pt paste pattern was put on a hotplate at 150 °C for 10 min to cure the paste. Then, it was sintered at 870 °C for 1 h (P330, Nabertherm GmbH, Bremen, Germany). To fabricate the sensing electrode, an oxide solutions with 14 wt% mass fraction of TiO_2 nanoparticles (diameter: 15 nm, Sigma Aldrich, MO, USA) were mixed up with anhydrous ethanol (99.7% purity, Sigma Aldrich, MO, USA) by magnetic stirring and acentric mixing process for 30 min. The second PVC film mask was used to pattern sensing electrode and mask the rest of the YSZ thin film surface. The TiO_2 nanoparticles solution was dropped onto the sensing electrode area (2.0 mm × 6.0 mm). Eventually, a thin film of 0.5 μm TiO_2 sensing film formed and was sintered at 500 °C for 30 min.
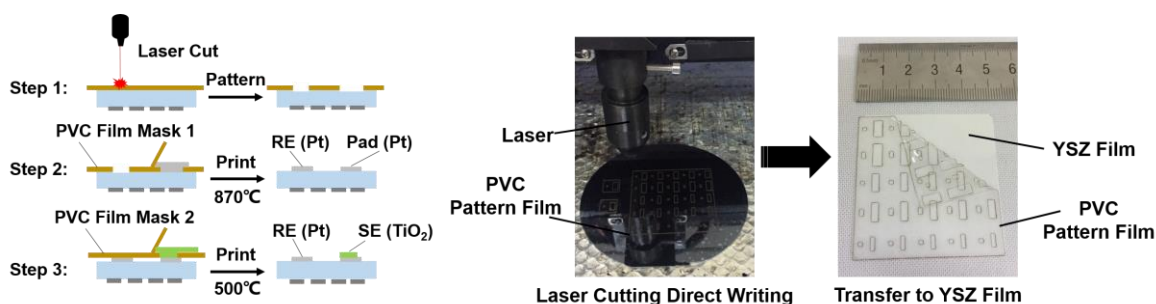

Figure 4. Schematic diagram of the fabrication process for the sensor's reference and sensing electrodes.

2.3. Electrical, Thermal, Surface Properties Characterization

Electrical and thermal properties of the NO_2 sensor were measured by a customized testing platform, as shown in Figure 5, including a digital multimeter, a DC power supply, an infrared imaging camera (Infra Tech VC HD Head 880, InfraTec, Dresden, Germany), a probe station and a semiconductor parameter analyzer (B1500A, Agilent, Santa Clara, CA, USA). The surface temperature profile of the NO_2 sensor was obtained and analyzed by the infrared image analyzing software (IRBIS3, InfraTec, Dresden, Germany). Surface properties of the sensor were characterized by scanning electron microscopy (Quanta 200, FEI, Hillsboro, OR, USA), with a detector enabling energy-dispersive X-ray spectroscopy analysis to characterize the thin film material for reference and sensing electrodes. Finally, the raw data will be processed by OriginLab software.
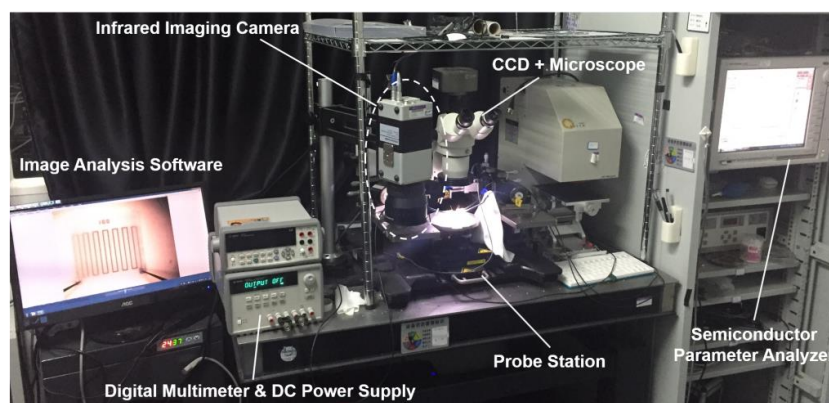

Figure 5. Testing platform for characterization of the sensor's electrothermal properties, including a digital multimeter, a DC power supply, an infrared imaging camera, a probe station and a semiconductor parameter analyzer.

2.4. Sensing Performance Characterization

The NO_2 gas sensing measurement was performed in a customized gas sensing and measurement platform. As shown in Figure 6, the testing system consists of a gas distribution module (0.15% NO_2/99.85% N_2), a gas chamber (15 L volume, humidity, flow rate adjustable), a detection and calibration system (PM80-X2, Eranntex, ShenZhen, China), and a data acquisition system (34461A Digit multimeter, Agilent, Santa Clara, CA, USA). The NO_2 sensor was powered by a DC power supply (E3633A, Agilent, Santa Clara, CA, USA). A digital thermocouple was used to monitor the surface temperature of the device in real time. Gas sensing experiment was carried out in a clean room with the humidity of 13% and environment temperature of 21.2 °C inside the gas chamber, with an oxygen concentration of 20.8% in a standard atmosphere.
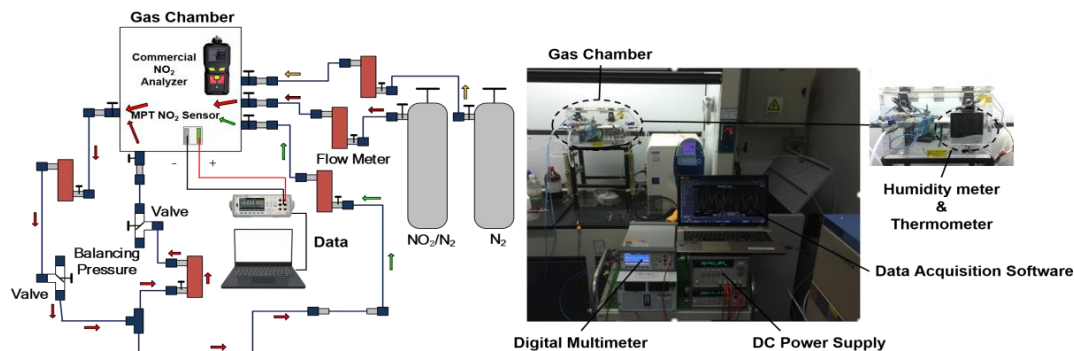

Figure 6. Testing platform for measuring the sensor's gas sensing performance.

3. Results and Discussion

A single NO_2 sensor based on a flexible YSZ ceramic film was shown in Figure 7, with the Pt reference electrode and the TiO_2 sensing electrode fabricated on the front side of the thin film, as well as the Ti/Pt heating electrode of 8.0 mm by 6.4 mm fabricated on the backside of the thin film. The heating electrode's width is measured as 102.2 µm on average, and the thickness of the heating electrode is measured as 4200 Å. As for the Pt reference electrode, its dimension is 2.1 mm by 5.9 mm, while TiO_2 sensing electrode's dimension is 2.2 mm by 6.1 mm.
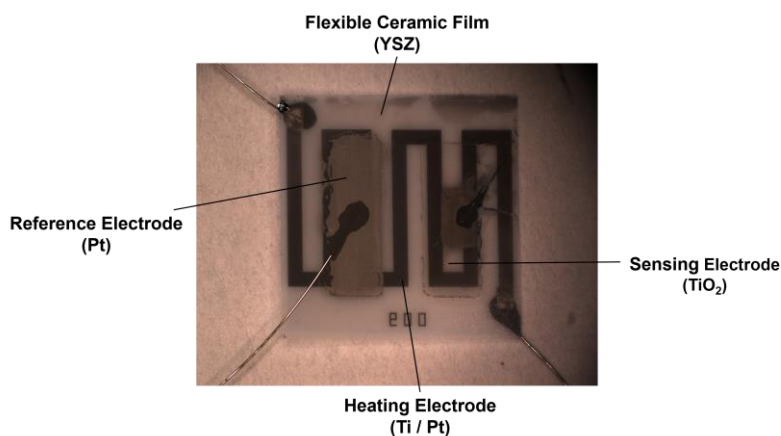

Figure 7. Optical image of a mixed-potential-type (MPT) sensor with a heating electrode, a reference electrode, an NO_2 sensing electrode on the back side and front side of a ultra-thin Y_2O_3-doped ZrO_2 (YSZ) ceramic film 20 µm thick.

The reference and sensing electrode surface profiles were characterized by scanning electron microscopy (SEM). As shown in Figure 8a, a porous Pt reference electrode was achieved by the shadow mask patterning method. Such a porous Pt surface with a porous size about several hundred nanometers will enable the rapid diffusion and permeation of oxygen and NO_2 gases on the electrode surface. For the sensing electrode, a mesoporous layer consisting of TiO_2 nanoparticles with a particle size of 10–20 nm formed after sintering treatment at 500 °C shown in Figure 8b and 8c. For the sensing electrode, homogenous anatase structured TiO_2 nanoparticles were achieved for NO_2 sensing as shown in Figure 8d. The thickness of the mesoporous TiO_2 layer is about 0.5 µm, as shown in Figure 8e. These uniform nanometer-sized pores will increase the contact area and absorption between NO_2 gas and the TiO_2 sensing material.

(**a**)

(**b**)

Figure 8. *Cont.*
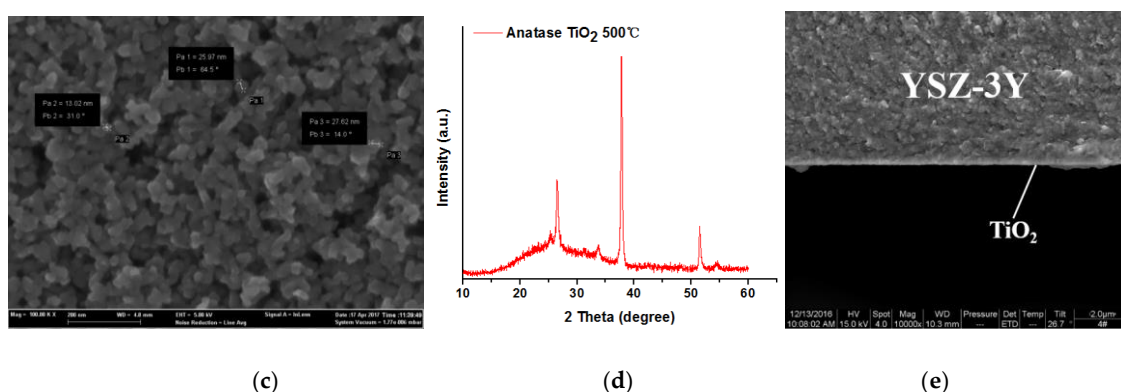
(c)　　　　　　　　　　　　　(d)　　　　　　　　　　　　　(e)
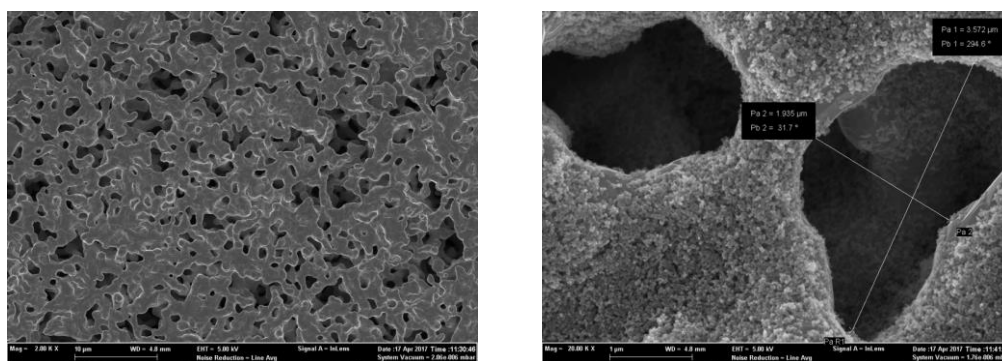
Figure 8. Scanning electron microscopy (SEM) image of (**a**) platinum reference electrode surface profile; (**b**) and (**c**) TiO$_2$ sensing electrode surface profile at 20,000 and 100,000 magnification; (**d**) X-ray diffraction (XRD) profile of anatase TiO$_2$ nanoparticles sintered at 500 °C; (**e**) SEM image of a cross section of YSZ thin film with the TiO$_2$ sensing material.

3.1. Electrothermal Properties of the NO$_2$ Sensor

The heating electrode's resistance is measured as 378 Ω in good accordance with the simulated result of 333 Ω. Comparing to the simulation result, an increase of the heating electrode's resistance is due to two factors: one is the decreased thickness of Ti/Pt film (4200 Å vs 4500 Å); the other is that thin film resistivity is typically higher than the material's bulk resistivity [23].

Simulated electrothermal properties of the NO$_2$ sensor and temperature profile on the thin YSZ film was demonstrated in Figure 9. Due to the low thermal conduction coefficient of the ceramic thin film (2.7 m^{-1}·K^{-1}), the temperature profile is not perfectly uniform inside the heating electrode region. Therefore, five regions of the NO$_2$ sensor were selected to investigate the electrothermal properties of the NO$_2$ sensor: (1) highest temperature region in the center; (2) reference electrode region; (3) sensing electrode region; and the two lowest temperature regions outside of the heating electrode.
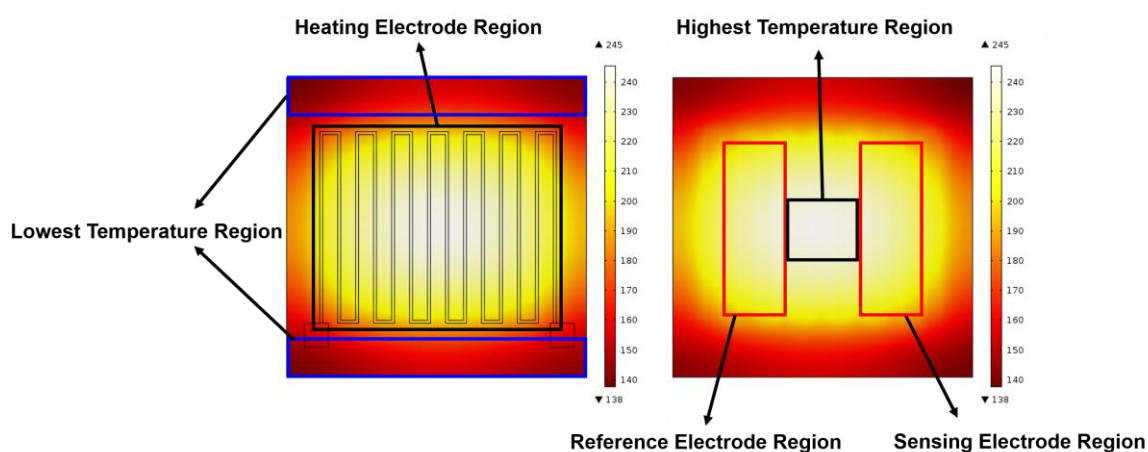

Figure 9. Surface temperature gradient distribution of the heating electrode by COMSOL simulation.

From the simulation results, as shown in Figure 10, it is derived and demonstrated that a uniform heating area is largely concentrated in the heating electrode area. To achieve the highest temperature of 245 °C in an area of 2.0 mm by 2.0 mm at the center of the heating electrode, the power consumption should be about 1512 mW. In the highest temperature region of 245 °C, the average temperate inside the heating electrode region is 214 °C. Outside the heating electrode, the average minimum temperature drops to 140 °C.
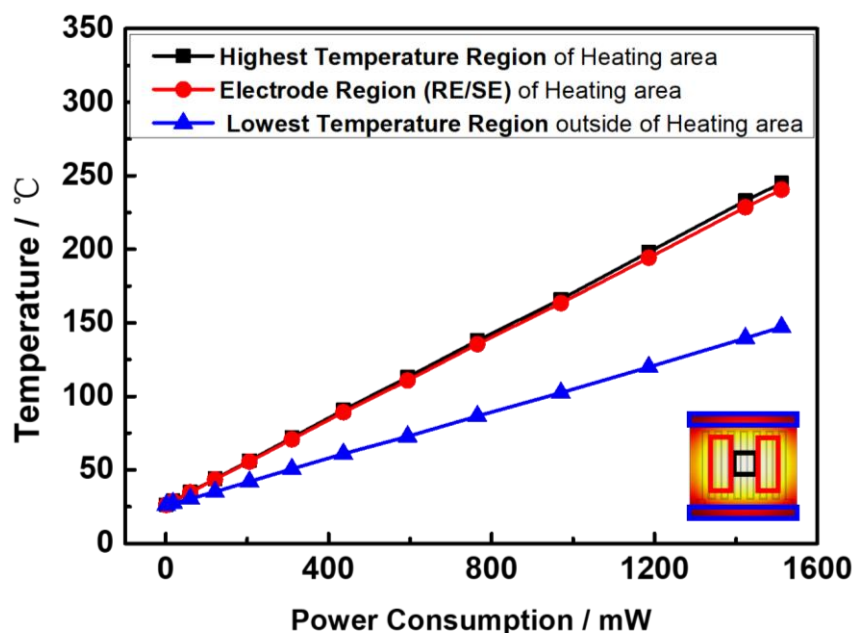
Figure 10. Working temperature vs. power consumption of the sensor by COMSOL simulation.

This phenomenon is verified by the corresponding experimental results in Figure 11. The temperature profile of the flexible NO_2 sensor measured by the infrared thermal imaging. To achieve the highest temperature of 246 °C in the center of the electrode (an area of 2.6 mm by 2.6 mm), the power consumption is about 1025 mW, in good accordance with the simulation results. The highest temperature of 246 °C was obtained by a heating power of 1025 mW. The average temperature inside the heating electrode region is 173 °C. Inside the reference and sensing electrode regions, the temperature range is from 150 °C to 240 °C. Outside the heating electrode region, the average temperature dropped to 110 °C and the minimum temperature of the sensor is 70 °C.

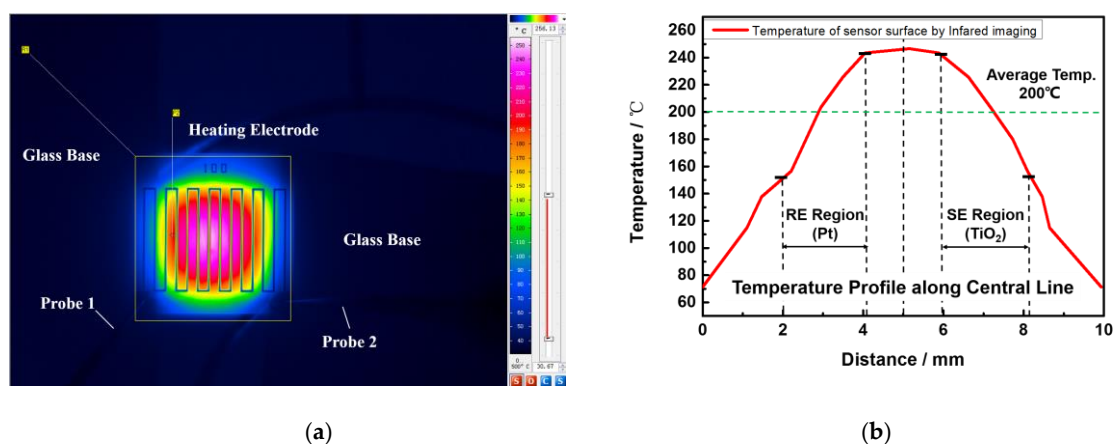(**a**)   (**b**)

Figure 11. Testing results of the sensor's surface temperature profile by the high-resolution infrared camera. (**a**) The sensor with an area of 10 mm × 10 mm with an applied voltage of 25 V; (**b**) Comparison of temperature profile along the sensor surface.

Comparing to our previous publications [24], power consumption is over 170 mW for an area of 0.36 mm^2 on a quartz substrate, and 1105 mW for an area of 0.36 mm^2 on a silicon substrate. Power assumption density of the flexible NO_2 sensor, 20 mW/mm^2, is about 1/20 of the power assumption density of the thin quartz gas sensor and 1/130 of the power assumption density of

the bulk silicon gas sensor. Low power consumption density is due to two factors: low thermal conductivity of YSZ thin film and ultra-thin thickness of the film. The thermal conductivity of YSZ thin film is 2.7 $W \cdot m^{-1} \cdot K^{-1}$, close to that of quartz material (1.2 $W \cdot m^{-1} \cdot K^{-1}$) and much smaller than that of silicon material (149 $W \cdot m^{-1} \cdot K^{-1}$). As for the thin film thickness, it is 20 microns and much smaller than those of the thin quartz wafer (100 μm) and the silicon wafer (500 μm) we used in our previous publication [25]. Low thermal conductivity with thin film thickness results in a low thermal mass of the ceramic film and leads to smaller power consumption density of the flexible NO_2 sensor.

3.2. NO_2 Sensing Performances

The sensor's response to NO_2 gas is demonstrated in Figure 12. Once the sensor was heated to a working temperature of 200 °C, 100 ppm NO_2 gas was delivered into the gas chamber. Then an electrochemical potential between the sensing electrode and the reference electrode was obtained as 26.0 mV. The sensor's response and recovery time are 10 s and 100 s, respectively. Comparing to existing publications [10,26], the working temperature of the flexible gas sensor is 200 °C smaller than most of the publications, and may be due to uniform and concentrated heating region resulted from the ultra-thin ceramic film, as well as the uniform porous reference and sensing electrodes surface [27]. It should be noted that there may exist an optimal working temperature for the sensor's sensitivity [28,29]. Higher temperature will lead to higher electrochemical potential induced by NO_2 reaction, as well as the electrochemical potential induced by O_2 reaction. Fluctuation of the electrochemical potential induced by O_2 reaction (background potential) may lower the sensor's NO_2 sensitivity. Further study on the relation between sensor's working temperature and sensitivity is underway.
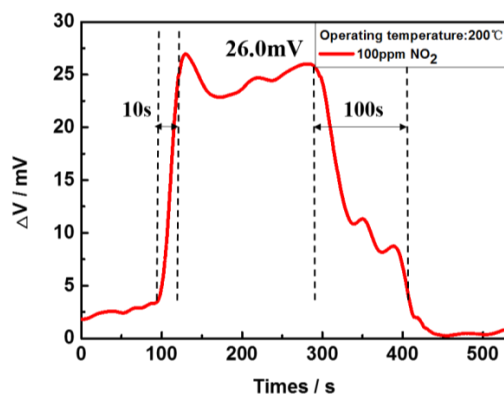

Figure 12. NO_2 sensing response for the flexible YSZ-3Y based sensor to the concentration of 100 ppm NO_2 at 200 °C.
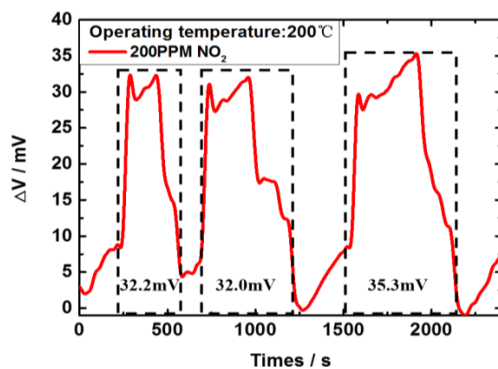

Figure 13. The sensor's gas sensing response for three cycles to 200 ppm NO_2 at a working temperature of 200 °C.

The NO$_2$ sensor's gas sensing repeatability is demonstrated in Figure 13 with alternating cycles of 200 ppm NO$_2$ at the working temperature of 200 °C. Though the response curves are not identical during the testing, the average peak sensing voltage is 26.0 mV, and the difference between the peak sensing voltage to 200 ppm NO$_2$ is 0.2 mV and 2.9 mV, demonstrating the sensor's capability to detect NO$_2$ emission.

The transient response of the NO$_2$ sensor tested at a concentration gradient from 0 to 500 ppm at 200 °C in 20% O$_2$ environment is shown in Figure 14. The response time tends to increase with the increasing of NO$_2$ concentrations. Response time (T$_r$), a time required to reach 90% of the steady-state value, was dependent on the NO$_2$ gas concentration. When tested at the concentration of NO$_2$ in the range of 0-300 ppm, Tr is smaller than 5 s. However, the sensor's response time (T$_r$) increases with the increase of the concentration of NO$_2$ from 300 to 500 ppm. The probable cause of this phenomenon is that the redox reaction on the sensing electrode surface will take some time and a higher concentration of NO$_2$ gas will decrease the active reaction sites on the sensing electrode surface in a short time. Once the first batch of NO$_2$ molecules finishes the absorption/desorption reaction, the NO$_2$ molecules followed up could not continue the redox reaction until the previous reactants finish the desorption process. Eventually, this phenomenon would result in a larger response time of the sensor at a high concentration of NO$_2$ gas. In addition, the NO$_2$ sensor works at a low temperature of 200 °C with a thin thickness of sensing electrode film (0.5 µm), and its sensing performance deteriorates at higher NO$_2$ concentration.
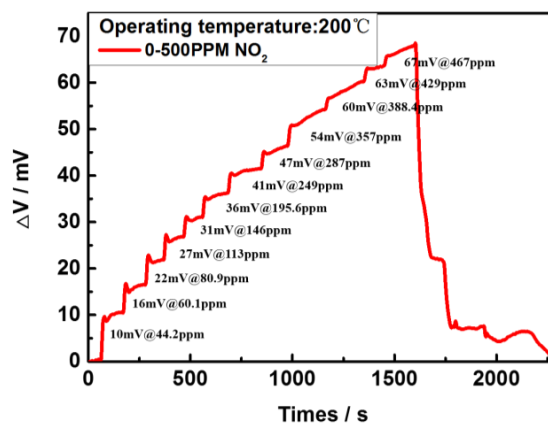

Figure 14. Gas sensing response of the sensor to NO$_2$ in the range from 0 ppm to 500 ppm at 200 °C.
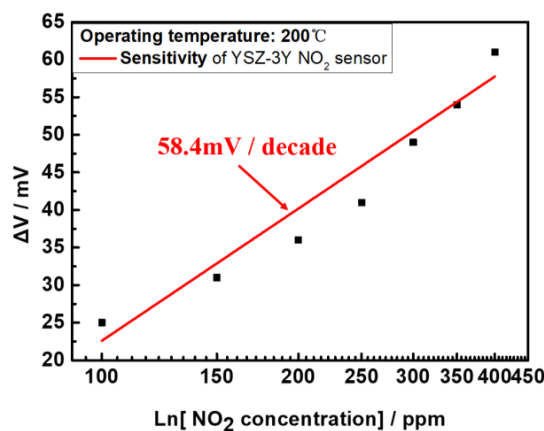

Figure 15. Gas sensing response to an NO$_2$ concentration from 100 to 500 ppm of the flexible MPT sensor.

As indicated in Figure 15, the sensing voltage of ΔV is linearly dependent on the logarithm of NO_2 concentration in the detected range conform to MPT mechanism at a working temperature of 200 °C [30,31]. The sensitivity of the sensor was derived as 58.4 mV/decade from the linear curve's slope, as well as a detection limit of 26.7 ppm. In addition, a variation of the oxygen concentration will affect the sensor response to NO_2 gas, as shown in Figure 16. We compared the sensing signals at different oxygen concentration, showing a variation of the output signal of 15%, similar to the phenomena described in other literature [21,32].
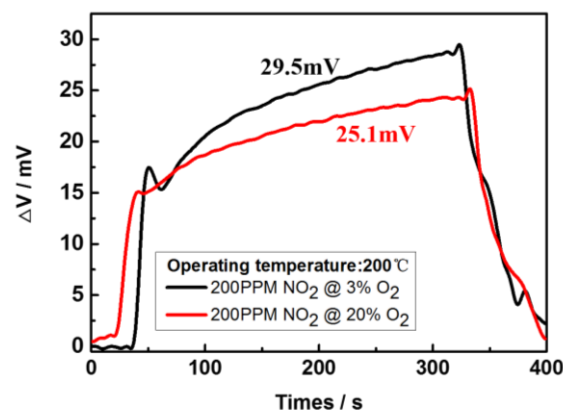

Figure 16. Responses of sensor to 200 ppm of NO_2 at different concentrations of O_2 at 200 °C.

3.3. Mechanical Stability of the NO_2 Sensor

The ultra-thin YSZ ceramic film's mechanical stability was characterized by measuring the film's bending strain. As shown in Figure 17a, a YSZ substrate of 20 μm thick was put in a bending stage with a fixed end and a moving end with an initial length of 1.18 cm. Once the YSZ substrate was compressed by pushing the moving end, the substrate's end-to-end length decreased to 0.81 cm. The substrate's bending radius R_{nom} can be calculated as 0.42 cm from Equation (1) [33,34]

$$R_{nom} = \frac{L}{2\pi \sqrt{\frac{dL}{L} - \frac{\pi^2 h_s^2}{12L^2}}} \tag{1}$$

where h_s is the YSZ substrate's thickness, 20 μm. L is the initial length of the YSZ substrate and dL is the decreased length of the substrate after compression. Additionally, the bending strain of the YSZ substrate ε_{nom} can be calculated as 2.38×10^{-3} from Equation (2)

$$\varepsilon_{nom} = h_s / (2R_{nom}) \tag{2}$$

Moreover, a series of bending fatigue experiments were carried out to investigate the mechanical stability of the sensor. As shown in Figure 18 a, the flexible YSZ-based NO_2 sensor was squeezed by two fingers to achieve a certain degree (about 30 degrees), bending to simulate the sensor's application and performance on a non-planar substrate. The sensor was tested at 100 ppm NO_2 concentration at 200 °C working temperature after 10, 20, 30, 40, and 50 times blending, respectively. The sensor's performance can be characterized by ΔV, which is described in Equation (3):

$$\Delta V = \frac{(\Delta V_n - \Delta V_0)}{\Delta V_0} \times 100 \tag{3}$$

where ΔV_n is sensing voltage difference of the sensor after n times of blending in the fatigue experiment. As indicated in Figure 18 b, the results show that the ΔV for the sensor at 100 ppm after 50 times was about 14.8%, which demonstrate the excellent mechanical stability of the flexible NO_2 sensor.
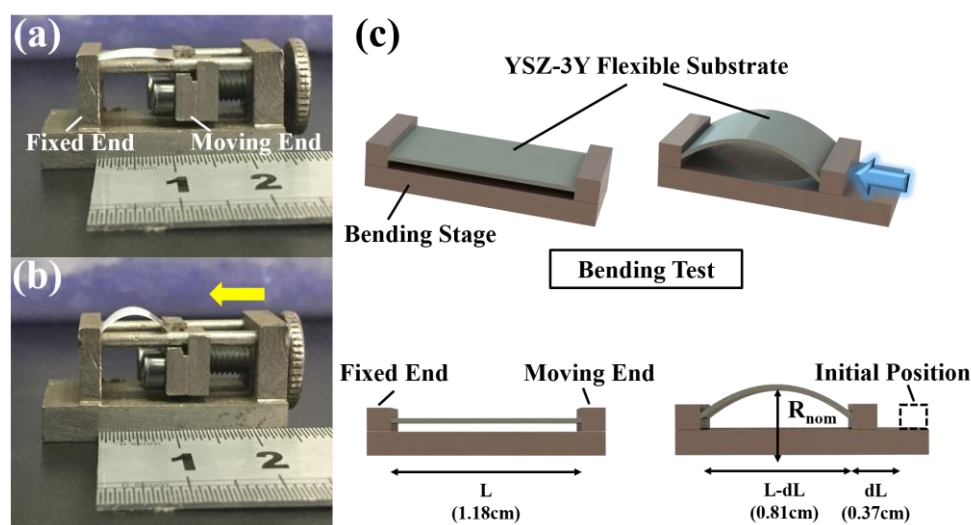
Figure 17. YSZ ceramic film's mechanical property measurement: (**a**) initial state of the YSZ substrate in the bending stage; (**b**) bending state of the YSZ substrate after compression; (**c**) schematic diagram of the bending test for measuring the substrate's bending radius and bending strain.
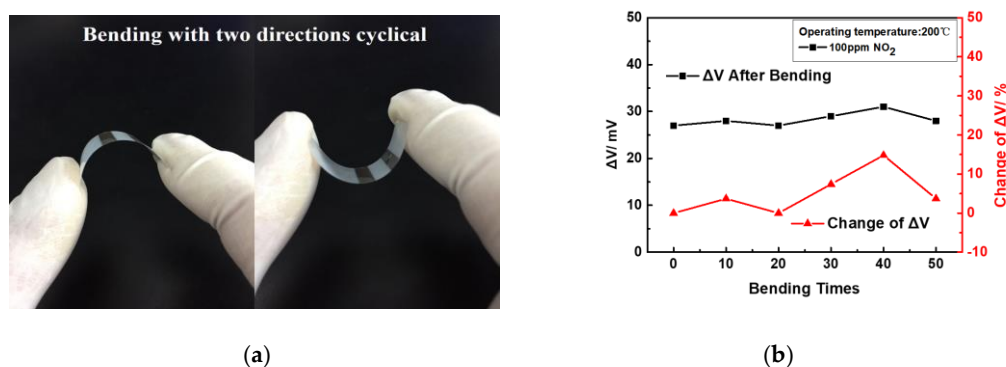

Figure 18. (**a**) Mechanical stability properties of sensor demonstrated in a bending fatigue experiment; (**b**) Mechanical and sensing stability performance after 10–50 times bending.

It should be noted that humidity in the ambient environment [10,35] and interference from other types of gases [15], such as NO, CO, and SO_2, are two critical parameters to affect the sensor's performance, and related research is underway.

4. Conclusions

A novel design and fabrication process for flexible MPT NO_2 sensors based on an ultra-thin YSZ ceramic film was reported. The sensor is composed of a heating electrode, a reference electrode, an NO_2 sensing electrode on the back side and front side of an ultra-thin 3 mol% Y_2O_3-doped ZrO_2 (YSZ-3Y) film 20 μm thick. The heating electrode was fabricated by a conventional lift-off process, while porous reference and sensing electrodes were fabricated by a two-step patterning method using shadow masks. Due to the ceramic film's low thermal conductivity and thin film thickness, a low power assumption of 1025 mW was applied to obtain a working temperature of 200 °C, in an area of 8.0 mm by 6.4 mm. The sensor's sensitivity could be achieved as 58.4 mV/decade at the working temperature of 200 °C. In addition, the flexible sensor demonstrates superior mechanical stability after bending over 50 times due to the mechanical stability of the YSZ ceramic film. These simply structured, but highly reliable flexible MPT NO_2 sensors may lead to wide application in the automobile industry for vehicle emission systems to reduce vehicle emissions and improve fuel efficiency.

Author Contributions: Rui You and Gaoshan Jing proposed the idea, proposed the simulation model. Rui You performed the simulation analysis and conducted the experiments with the aid of Hongyan Yu. Rui You and Gaoshan Jing prepared the manuscript. Tianhong Cui is the supervisor of the research and proposed the research topic.

Conflicts of Interest: The authors declare no conflict of interest.

References

1. Schmale, J. Clean up our skies. *Nature* **2014**, *515*, 335–337. [CrossRef] [PubMed]

2. Moos, R.; Reetmeyer, B.; Hürland, A.; Plog, C. Sensor for directly determining the exhaust gas recirculation rate—EGR sensor. *Sens. Actuators B Chem.* **2006**, *119*, 57–63. [CrossRef]

3. Afzal, A.; Cioffi, N.; Sabbatini, L.; Torsi, L. Nox sensors based on semiconducting metal oxide nanostructures: Progress and perspectives. *Sens. Actuators B Chem.* **2012**, *171–172*, 25–42. [CrossRef]

4. Fleischer, M.; Simon, E.; Rumpel, E.; Ulmer, H.; Harbeck, M.; Wandel, M.; Fietzek, C.; Weimar, U.; Meixner, H. Detection of volatile compounds correlated to human diseases through breath analysis with chemical sensors. *Sens. Actuators B Chem.* **2002**, *83*, 245–249. [CrossRef]

5. Qu, F.; He, B.; Guarecuco, R.; Yang, M. Mesoporous WN/WO_3-composite nanosheets for the chemiresistive detection of NO_2 at room temperature. *Inorganics* **2016**, *4*, 24. [CrossRef]

6. Groß, A.; Richter, M.; Kubinski, D.J.; Visser, J.H.; Moos, R. The effect of the thickness of the sensitive layer on the performance of the accumulating NO_x sensor. *Sensors* **2012**, *12*, 12329–12346. [CrossRef]

7. Razeghi, M.; Yu, Y.; Sanchez, N.P.; Lou, M.; Zheng, C.; Wu, H.; Głuszek, A.K.; Hudzikowski, A.J.; Griffin, R.J.; Tittel, F.K. CW DFB-QCL- and EC-QCL-Based Sensor for Simultaneous NO and NO_2 Measurements via Frequency Modulation Multiplexing Using Multi-Pass Absorption Spectroscopy. Available online: https://scholarship.rice.edu/handle/1911/93857 (accessed on 27 July 2017).

8. Chen, X.; Yang, C.; Hu, M.; Xu, Z.; Fan, X.; Wei, M.; Yao, L.; He, Y.; Kan, R. High Sensitivity Measurement of NO, NO_2 and NH_3 Using MIR-QCL and Time Division Multiplexing WMS Technology. Available online: http://proceedings.spiedigitallibrary.org/proceeding.aspx?articleid=2577479 (accessed on 27 July 2017).

9. Elumalai, P.; Wang, J.; Zhuiukov, S.; Terada, D.; Hasei, M.; Miura, N. Sensing characteristics of YSZ-based mixed-potential-type planar NO_x sensors using NiO sensing electrodes sintered at different temperatures. *Electrochem. Soc.* **2005**, *152*, H95–H101. [CrossRef]

10. Liu, F.; Wang, B.; Yang, X.; Guan, Y.; Sun, R.; Wang, Q.; Liang, X.; Sun, P.; Lu, G. High-temperature stabilized zirconia-based sensors utilizing $MNb_2 O_6$ (M: Co, Ni and Zn) sensing electrodes for detection of NO_2. *Sens. Actuators B Chem.* **2016**, *232*, 523–530. [CrossRef]

11. Diao, Q.; Yin, C.; Liu, Y.; Li, J.; Gong, X.; Liang, X.; Yang, S.; Chen, H.; Lu, G. Mixed-potential-type NO_2 sensor using stabilized zirconia and Cr_2O_3-WO_3 nanocomposites. *Sens. Actuators B Chem.* **2013**, *180*, 90–95. [CrossRef]

12. Miura, N.; Nakatou, M.; Zhuiykov, S. Development of NO_x sensing devices based on YSZ and oxide electrode aiming for monitoring car exhausts. *Ceram. Int.* **2004**, *30*, 1135–1139. [CrossRef]

13. Romanytsia, I.; Viricelle, J.P.; Vernoux, P.; Pijolat, C. Application of advanced morphology Au–X (X=YSZ, ZrO_2) composites as sensing electrode for solid state mixed-potential exhaust NO_x sensor. *Sens. Actuators B Chem.* **2015**, *207*, 391–397. [CrossRef]

14. Yoo, J.; Chatterjee, S.; Wachsman, E.D. Sensing properties and selectivities of a WO_3/YSZ/Pt potentiometric nox sensor. *Sens. Actuators B Chem.* **2007**, *122*, 644–652. [CrossRef]

15. Mahendraprabhu, K.; Elumalai, P. Stabilized zirconia-based selective NO_2 sensor using sol-gel derived Nb_2O_5 sensing-electrode. *Sens. Actuators B Chem.* **2017**, *238*, 105–110. [CrossRef]

16. Sun, X.; Zhang, C.; Feng, T.; Jiang, D. Sensing behavior of mixed potential NO_2 sensors equipped with $LaMO_3$ (M = Fe or Cr) sensing electrodes. *Ionics* **2014**, *21*, 1725–1730. [CrossRef]

17. Lu, G.; Miura, N.; Yamazoe, N. High-temperature hydrogen sensor based on stabilized zirconia and a metal oxide electrode. *Sens. Actuators B Chem.* **1996**, *35–36*, 130–135. [CrossRef]

18. Cai, H.; Sun, R.; Yang, X.; Liang, X.; Wang, C.; Sun, P.; Liu, F.; Zhao, C.; Sun, Y.; Lu, G. Mixed-potential type nox sensor using stabilized zirconia and MoO_3–In_2O_3 nanocomposites. *Ceram. Int.* **2016**, *42*, 12503–12507. [CrossRef]

19. Liu, F.; Guan, Y.; Dai, M.; Zhang, H.; Guan, Y.; Sun, R.; Liang, X.; Sun, P.; Liu, F.; Lu, G. High performance mixed-potential type NO_2 sensors based on three-dimensional TPB and $Co_3V_2O_8$ sensing electrode. *Sens. Actuators B Chem.* **2015**, *216*, 121–127. [CrossRef]

20. Liang, X.; Yang, S.; Li, J.; Zhang, H.; Diao, Q.; Zhao, W.; Lu, G. Mixed-potential-type zirconia-based NO_2 sensor with high-performance three-phase boundary. *Sens. Actuators B Chem.* **2011**, *158*, 1–8. [CrossRef]

21. Wang, B.; Liu, F.; Yang, X.; Guan, Y.; Ma, C.; Hao, X.; Liang, X.; Liu, F.; Sun, P.; Zhang, T.; et al. Fabrication of well-ordered three-phase boundary with nanostructure pore array for mixed potential-type zirconia-based NO_2 sensor. *ACS Appl. Mater. Interfaces* **2016**, *8*, 16752–16760. [CrossRef] [PubMed]

22. Thin E—Strate Material Properties. Available online: https://www.enrg-inc.com/documents/Material% 20Property%20Table%20V2%202015.pdf (accessed on 27 July 2017).

23. Zhai, Y.; Cai, C.; Huang, J.; Liu, H.; Zhou, S.; Liu, W. Study on the resistance characteristic of Pt thin film. *Phys. Proced.* **2012**, *32*, 772–778. [CrossRef]

24. Lu, W.; Jing, G.; Bian, X.; Yu, H.; Cui, T. A quartz-based micro catalytic methane sensor by high resolution screen printing. *J. Micromech. Microeng.* **2016**, *26*, 025021. [CrossRef]

25. Lu, W.; Jing, G.; Bian, X.; Yu, H.; Cui, T. Micro catalytic methane sensors based on 3D quartz structures with cone-shaped cavities etched by high-resolution abrasive sand blasting. *Sens. Actuators A Phys.* **2016**, *242*, 9–17. [CrossRef]

26. Miura, N.; Sato, T.; Anggraini, S.A.; Ikeda, H.; Zhuiykov, S. A review of mixed-potential type zirconia-based gas sensors. *Ionics* **2014**, *20*, 901–925. [CrossRef]

27. Milton, O. *Materials Science of Thin Films*; Academic Press: San Diego, CA, USA, 2002.

28. Giang, H.T.; Duy, H.T.; Ngan, P.Q.; Thai, G.H.; Thu, D.T.A.; Thu, D.T.; Toan, N.N. High sensitivity and selectivity of mixed potential sensor based on $Pt/YSZ/SMFeO_3$ to NO_2 gas. *Sens. Actuators B Chem.* **2013**, *183*, 550–555. [CrossRef]

29. Tho, N.D.; Van Huong, D.; Ngan, P.Q.; Thai, G.H.; Thu, D.T.A.; Thu, D.T.; Tuoi, N.T.M.; Toan, N.N.; Giang, H.T. Effect of sintering temperature of mixed potential sensor $Pt/YSZ/LaFeO_3$ on gas sensing performance. *Sens. Actuators B Chem.* **2016**, *224*, 747–754. [CrossRef]

30. Guth, U.; Zosel, J. Electrochemical solid electrolyte gas sensors -hydrocarbon and nox analysis in exhaust gases. *Ionics* **2004**, *10*, 366–377. [CrossRef]

31. Liu, F.; Guan, Y.; Sun, H.; Xu, X.; Sun, R.; Liang, X.; Sun, P.; Gao, Y.; Lu, G. Ysz-based NO_2 sensor utilizing hierarchical In_2O_3 electrode. *Sens. Actuators B Chem.* **2016**, *222*, 698–706. [CrossRef]

32. Liu, F.; Wang, B.; Yang, X.; Guan, Y.; Wang, Q.; Liang, X.; Sun, P.; Wang, Y.; Lu, G. High-temperature NO_2 gas sensor based on stabilized zirconia and $CoTa_2O_6$ sensing electrode. *Sens. Actuators B Chem.* **2017**, *240*, 148–157. [CrossRef]

33. Park, S.-I.; Ahn, J.-H.; Feng, X.; Wang, S.; Huang, Y.; Rogers, J.A. Theoretical and experimental studies of bending of inorganic electronic materials on plastic substrates. *Adv. Funct. Mater.* **2008**, *18*, 2673–2684. [CrossRef]

34. Dai, L.; Feng, X.; Liu, B.; Fang, D. Interfacial slippage of inorganic electronic materials on plastic substrates. *Appl. Phys. Lett.* **2010**, *97*, 221903. [CrossRef]

35. Petrila, I.; Popa, K.; Tudorache, F. Microstructure, electrical and humidity sensing properties of light rare earths zirconates. *Sens. Actuators A Phys.* **2016**, *247*, 156–161. [CrossRef]